

## Description of isospin mixing by a generator coordinate method

M. Kimura\*

*Department of Physics, Hokkaido University, Sapporo 060-0810, Japan;  
Nuclear Reaction Data Centre, Hokkaido University, Sapporo 060-0810, Japan;  
and RIKEN Nishina Center, Wako, Saitama 351-0198, Japan*

Y. Suzuki

*Department of Physics, Hokkaido University, Sapporo 060-0810, Japan*

T. Baba

*Kitami Institute of Technology, Kitami 090-8507, Japan*

Y. Taniguchi 

*Department of Information Engineering, National Institute of Technology (KOSEN), Kagawa College, Mitoyo 769-1192, Japan  
and Research Center for Nuclear Physics (RCNP), Osaka University, Ibaraki 567-0047, Japan*

 (Received 17 August 2021; revised 25 October 2021; accepted 7 January 2022; published 18 January 2022)

**Background:** Isospin mixing is an interesting feature of atomic nuclei that plays a crucial role in the astrophysical nuclear reactions. However, variational nuclear structure models cannot describe it in a straightforward manner.

**Purpose:** We propose a tractable method to describe isospin mixing within the framework of a generator coordinate method and demonstrate its usability.

**Method:** We generate basis wave functions by applying the Fermi transition operator to the wave functions of isobars. The superposition of these basis wave functions and variationally obtained wave functions quantitatively describes isospin mixing.

**Results:** We apply our method to  $^{14}\text{N}$  and show that it reasonably describes both  $T = 0$  and 1 states and their mixing. The energy spectrum and  $E1$  transition strengths are compared with the experimental data.

**Conclusion:** The proposed method is effective in describing isospin mixing and is particularly useful for discussing of  $\alpha$ -capture reactions of  $N = Z$  nuclei.

DOI: [10.1103/PhysRevC.105.014311](https://doi.org/10.1103/PhysRevC.105.014311)

### I. INTRODUCTION

Isospin symmetry is a fundamental symmetry of the strong interaction and nuclear force. Because of this symmetry, isobars share a group of states having the same total isospin, which are called isobaric analog states [1,2]. For example, the  $N = Z$  nucleus  $^{14}\text{N}$  has  $T = 1$  states such as the  $0_1^+$  state at 2.31 MeV and the  $1_2^-$  state at 8.06 MeV which are the isobaric analog states corresponding to the ground and first excited states, respectively, of  $^{14}\text{C}$  and  $^{14}\text{O}$ .

In reality, isospin is an approximate symmetry of atomic nuclei due to the symmetry-breaking terms of nuclear force and Coulomb interaction. Consequently, the mixing of states with different isospins (isospin mixing) occurs especially in excited states. The above-mentioned  $1_2^-$  state of  $^{14}\text{N}$  is a well-known example of isospin mixing for which the admixture of the  $T = 0$  and 1 components has been experimentally confirmed [3,4].

Isospin mixing has an interesting side effect on the selection rule of  $E1$  transitions [1]. At the first order of the long-wavelength approximation, the  $E1$  transition operator is purely an isovector, and hence, the transition between two  $T = 0$  states is strictly forbidden. The higher-order isoscalar term potentially contributes to the transition, but the contribution has been confirmed to be minor [5]. However, isospin mixing causes small contamination of the  $T = 1$  component, which allows the transition. This  $E1$  transition enabled by isospin mixing occasionally plays a crucial role in astrophysical reactions [6,7]. The radiative  $\alpha$ -capture reactions of  $N = Z$  nuclei such as  $^{12}\text{C}(\alpha, \gamma)^{16}\text{O}$  and  $^{16}\text{O}(\alpha, \gamma)^{20}\text{Ne}$  [5,8,9] are well-known examples for such reactions. Isospin mixing increases the reaction rate and can affect the evolution of stars and the abundance of the elements.

Thus, the isospin mixing in  $N = Z$  nuclei is an interesting issue relevant to astronomical nuclear reactions. However, the descriptions of the isobaric analog states and isospin mixing are not straightforward for variational models such as Hartree-Fock models. Since the  $T = 0$  states are usually more deeply bound than the  $T = 1$  states, the energy variation yields only

\*masaaki@nucl.sci.hokudai.ac.jp

the  $T = 0$  states, and the  $T = 1$  states are hardly obtained. To overcome this problem, several methods and prescriptions have been proposed [10–13]. For example, isospin projection before the variation [14,15] is a solid approach to solving this problem but computationally demanding. Therefore, the development of a simpler but accurate method is desirable.

In this paper, we propose a tractable method to describe isobaric analog states and isospin mixing within the framework of a generator coordinate method (GCM). We generate the basis wave functions by applying the Fermi transition operator to the wave functions of isobars. Using  $^{14}\text{N}$  as an example, we show that the superposition of the generated wave functions and variationally obtained wave functions quantitatively describes both the  $T = 0$  and 1 states and isospin mixing.

In the next section, we introduce a method to describe isobaric analog states and isospin mixing. In Sec. III, we present numerical results for the  $T = 0$  and 1 states and their mixing in  $^{14}\text{N}$ . The last section summarizes this work.

## II. THEORETICAL FRAMEWORK

### A. Hamiltonian and variational wave function

We use the  $A$ -body Hamiltonian given as

$$H = - \sum_i^A \frac{\hbar^2 \nabla_i^2}{2m_N} - t_{\text{c.m.}} + \sum_{i < j}^A v_{NN}(ij) + \sum_{i < j}^Z v_C(ij), \quad (1)$$

where the Gogny D1S density functional [16] is used as an effective nucleon-nucleon interaction ( $v_{NN}$ ) and the proton-neutron mass difference is ignored. In other words, we consider only the Coulomb interaction as the source of isospin symmetry breaking. This simplification may be validated in the case of  $^{14}\text{N}$ , which we will discuss later, because the Coulomb interaction should dominate over other symmetry-breaking terms.

The variational wave function is a parity-projected Slater determinant,

$$\Phi^\pi = \hat{P}^\pi \mathcal{A}\{\varphi_1 \varphi_2 \dots \varphi_A\}, \quad \pi = \pm, \quad (2)$$

where  $\hat{P}^\pi$  is the parity projection operator. The single-particle wave packet  $\varphi_i$  is represented by a deformed Gaussian [17],

$$\varphi_i(\mathbf{r}) = \prod_{\sigma=x,y,z} e^{-v_\sigma (r_\sigma - Z_{i\sigma})^2} \chi_i \eta_i, \quad (3)$$

$$\chi_i = a_i \chi_\uparrow + b_i \chi_\downarrow, \quad \eta_i = \{\text{proton or neutron}\}. \quad (4)$$

The variational parameters are the width ( $v_x, v_y, v_z$ ) and the centroids  $\mathbf{Z}_i$  of Gaussian wave packets as well as spin directions  $a_i$  and  $b_i$ . They are determined by energy variation with a constraint on the matter quadrupole deformation parameter  $\beta$ . We denote the wave function obtained with the energy variation as  $\Phi^\pi(\beta)$ , which has the minimum energy for a given value of the parameter  $\beta$ . As expressed in Eq. (2) and (4), the antisymmetrized molecular dynamics (AMD) wave function is not an eigenstate of isospin but an eigenstate of charge (fixed proton and neutron numbers). Therefore, in general, it describes an isospin-mixed state. However, the energy variation tends to yield the minimum isospin state as it is

energetically favored. In short, the energy variation produces wave functions dominated by the  $T = 0$  component for  $^{14}\text{N}$  and those dominated by the  $T = 1$  component for  $^{14}\text{C}$ .

### B. Basis wave functions for isobaric analog states

As explained above, it is not straightforward to obtain the wave functions of isobaric analog states, e.g., the  $T = 1$  states of  $^{14}\text{N}$ , through the energy variation. Here, we propose a simple method to generate the basis wave functions for describing the isobaric analog states. Let us explain it by taking the  $T = 1$  states of  $^{14}\text{N}$  as examples. Suppose that we have obtained the wave function of  $^{14}\text{C}$  through the energy variation as follows:

$$\Phi^\pi(\beta, ^{14}\text{C}(T \simeq 1)) = P^\pi \mathcal{A}\{\varphi_1 \dots \varphi_6 \varphi_7 \dots \varphi_{14}\}, \quad (5)$$

where  $\varphi_1 \dots \varphi_6$  and  $\varphi_7 \dots \varphi_{14}$  are the proton and neutron single-particle wave packets, respectively. Note that this wave function is mainly composed of the  $T = 1$  component (minimum isospin for  $^{14}\text{C}$ ). Then, we simply apply the Fermi transition operator of  $\beta^-$  decay to produce the wave function of  $^{14}\text{N}$ :

$$\begin{aligned} \Phi^\pi(\beta, ^{14}\text{N}(T \simeq 1)) &= T^+ \Phi^\pi(\beta, ^{14}\text{C}(T \simeq 1)) \\ &= \sum_{i=7}^{14} P^\pi \mathcal{A}\{\varphi_1 \dots \varphi_6 \varphi_7 \dots \varphi_i \dots \varphi_{14}\}, \end{aligned} \quad (6)$$

where the  $i$ th neutron wave packet ( $i = 7, \dots, 14$ ) is converted into a proton. Since  $T^+$  commutes with  $T^2$ , this wave function approximates the isobaric analog state ( $T = 1$  states) of  $^{14}\text{N}$ . We propose the use of each term of Eq. (6) as the basis wave function for GCM. Thus, we generate eight wave functions for  $^{14}\text{N}$  from a single  $^{14}\text{C}$  wave function, which are denoted as follows:

$$\begin{aligned} \Phi_i^\pi(\beta, ^{14}\text{N}(T \simeq 1)) &= t_i^+ \Phi^\pi(\beta, ^{14}\text{C}(T \simeq 1)) \\ &= P^\pi \mathcal{A}\{\varphi_1 \dots \varphi_6 \varphi_7 \dots \varphi_i \dots \varphi_{14}\}. \end{aligned} \quad (7)$$

### C. Generator coordinate method

Once the basis wave functions are prepared, we perform angular-momentum projection and GCM calculation. The basis wave functions are projected to the eigenstates of the angular momentum and superposed as follows:

$$\begin{aligned} \Psi_M^{J\pi} &= \sum_{\beta K} f_{\beta K} P_{MK}^J \Phi^\pi(\beta, ^{14}\text{N}(T \simeq 0)) \\ &+ \sum_{\beta Ki} g_{\beta Ki} P_{MK}^J \Phi_i^\pi(\beta, ^{14}\text{N}(T \simeq 1)), \end{aligned} \quad (8)$$

where  $P_{MK}^J$  is the angular-momentum projection operator. Note that  $\Phi^\pi(\beta, ^{14}\text{N}(T \simeq 0))$  are obtained through the energy variation and mainly consist of  $T = 0$  component, whereas  $\Phi_i^\pi(\beta, ^{14}\text{N}(T \simeq 1))$  are generated by Eq. (7) and mainly consist of the  $T = 1$  component. The eigenenergies and the coefficients of superposition  $f_{\beta K}$  and  $g_{\beta Ki}$  are determined by solving the Hill-Wheeler equation [18].

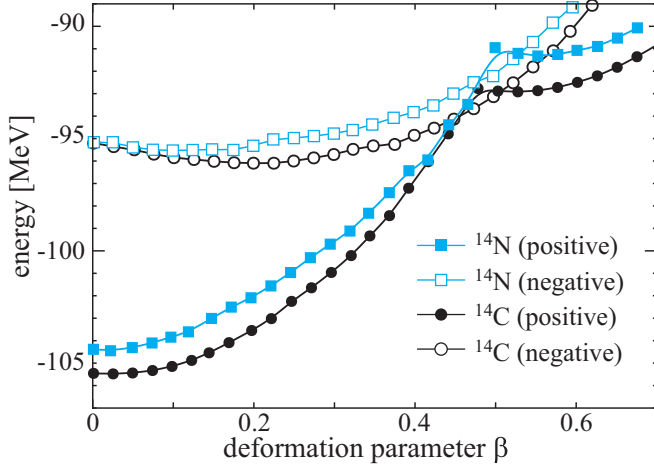


FIG. 1. Energy curves for  $^{14}\text{N}$  and  $^{14}\text{C}$  as functions of the quadrupole deformation parameter  $\beta$  obtained through the energy variation after parity projection.

### III. RESULTS AND DISCUSSION

Figure 1 shows the energy curves of  $^{14}\text{N}$  and  $^{14}\text{C}$  as functions of the quadrupole deformation parameter  $\beta$ , which are obtained through the energy variation after parity projection. The positive-parity states have a spherical energy minimum with the  $N = 8$  closed shell for  $^{14}\text{C}$  and a single neutron hole for  $^{14}\text{N}$ , which are the dominant components of the ground states. As quadrupole deformation grows, the energy increases rapidly, and level crossing occurs, creating an energy plateau around  $\beta = 0.6$ . In this plateau, both nuclei have two-particle and two-hole ( $2p2h$ ) configurations, which generate highly excited states [19,20]. The negative-parity energy curves are located at a much higher energy than the positive-parity states as they involve particle-hole excitation across the  $N = Z = 8$  shell gap. The particle-hole configuration changes from  $1p1h$  to  $3p3h$  at  $\beta = 0.5$ , where both  $^{14}\text{N}$  and  $^{14}\text{C}$  have a kink in the energy curve. Thus,  $^{14}\text{N}$  and  $^{14}\text{C}$  have energy curves with similar behaviors due to the similarity in the single-particle configurations. The energy difference between  $^{14}\text{N}$  and  $^{14}\text{C}$  is due to the difference in the the isospin channel ( $T = 0$  for  $^{14}\text{N}$  and  $T = 1$  for  $^{14}\text{C}$ ) and the Coulomb interaction.

As explained in the previous section, we apply the Fermi transition operator of  $\beta^-$  decay to the wave functions of  $^{14}\text{C}$  (circles in Fig. 1) to yield the wave functions of  $^{14}\text{N}$  with  $T = 1$ . The wave functions thus generated are superposed with the wave functions of  $^{14}\text{N}$  with  $T = 0$  (squares in Fig. 1) to perform the GCM calculations.

The spectra of  $^{14}\text{N}$  obtained from the GCM calculations are shown in Fig. 2. By using only the variationally obtained wave functions of  $^{14}\text{N}$  (without the  $T = 1$  wave functions generated from  $^{14}\text{C}$ ), the GCM calculation (blue lines in Fig. 2) fails to reproduce several excited states such as the  $0^+_{1,2}$ ,  $0^-_2$ , and  $1^-_2$  states, all of which are  $T = 1$  states. Thus, the variational calculations energetically favor the  $T = 0$  states and leave out the  $T = 1$  states. On the contrary, by adding the basis wave functions generated by applying the Fermi transition operator to the  $^{14}\text{C}$  wave functions, the present model plausibly de-

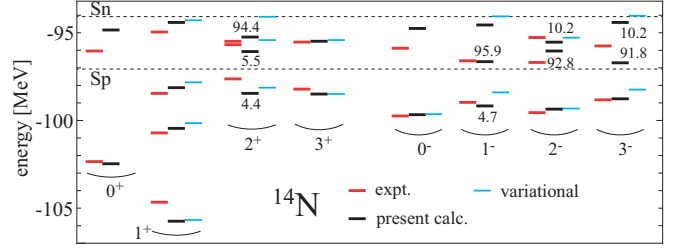


FIG. 2. Calculated and observed level scheme of  $^{14}\text{N}$  up to  $J^\pi \leq 3^\pm$ . Black lines show the result of the present model, whereas blue lines show the results calculated using only the variationally obtained basis wave functions. The numbers in the figure indicate the amount of the  $T = 1$  component in percentage for the states with sizable isospin mixing.

scribes both the  $T = 0$  and 1 states (black lines). Note that all the observed states up to  $E_x < 10$  MeV are reasonably reproduced by our simple method, although the calculation slightly overestimates the binding energy of the ground state. To elucidate the accuracy of the present calculations, Table I lists the electromagnetic properties of the  $1^+_{1,2}$  ( $T = 0$ ) and  $0^+_1$  ( $T = 1$ ) states. It is encouraging that the present calculation reproduces not only the electromagnetic moments of the individual states but also the transition probabilities between the  $T = 0$  and 1 states [21]. Thus, our proposed method is simple but accurately describes both the  $T = 0$  and 1 states with a small computational cost.

Now, we discuss the isospin mixing. The present calculation yielded several states with sizable isospin mixing larger than 4%, for which the mixing ratios (amount of the  $T = 1$  component) are in Table II and in Fig. 2. Table II indicates that the conventional method of determining the wave functions through energy variation does not yield strong isospin mixing; the resulting isospin mixing is at most 4% even in the highly excited state. On the other hand, our proposed method, which explicitly mixes  $T \simeq 0$  and  $T \simeq 1$ , yields much stronger mixing. We also note that the states close to the  $^{13}\text{C} + p$  or  $^{13}\text{N} + n$

TABLE I. Calculated and observed [21–23] properties of the low-lying  $1^+$  and  $0^+$  states. The excitation energy, magnetic dipole moment, and electric quadrupole moment are given in units of MeV,  $\mu_N$ , and  $\text{fm}^2$ , respectively. The reduced transition probabilities of  $M1$  and  $E2$  are given in Weisskopf units.

$J^\pi$	$E_x$		$\mu$		$Q$	
	calc.	exp.	calc.	exp.	calc.	exp. [23]
$1^+_1 (T = 0)$	0.0	0.0	0.39	0.40	1.7	2.0
$1^+_2 (T = 0)$	4.9	3.9	0.80	—	0.45	—
$0^+_1 (T = 1)$	3.2	2.3	—	—	—	—
	$B(M1)$		$B(E2)$			
$J^\pi_i \rightarrow J^\pi_f$	calc.	exp.	calc.	exp.		
$0^+_1 \rightarrow 1^+_1$	0.023	0.026(1)	—	—		
$1^+_2 \rightarrow 0^+_1$	1.2	1.0(3)	—	—		
$1^+_2 \rightarrow 1^+_1$	$1.4 \times 10^{-4}$	$3.3(13) \times 10^{-4a}$	2.7	2.1(8) <sup>a</sup>		

<sup>a</sup>Calculated from the lifetime [21] and the  $E2/M1$  mixing ratio [22].

TABLE II. Amount of the  $T = 1$  component in percentage obtained using the conventional variational AMD method and the present GCM. The states that have a mixing ratio larger than 4% or smaller than 96% are listed.

$J^\pi$	variational	present
$2_1^+$	1.2	4.4
$2_2^+$	2.1	5.5
$2_3^+$	–	94.4
$1_1^-$	0.8	4.7
$1_2^-$	–	95.9
$2_2^-$	–	92.8
$2_3^-$	3.4	10.2
$3_2^-$	–	91.8
$3_3^-$	3.3	10.2

threshold energies have strong isospin mixing, which is related to the origin of the isospin mixing as explained below.

Among these states, the  $1_1^-$  (5.69 MeV,  $T = 0$ ) and  $1_2^-$  (8.06 MeV,  $T = 1$ ) states are a well-known example of isospin mixing, and their mixing ratio was evaluated experimentally [4]. In the following, we discuss how these states are described by our model and analyze their structure. Table III lists the electric and magnetic dipole transition probabilities of these  $1^-$  states. Here, we have neglected the higher-order isoscalar term of the  $E1$  operator as its effect is known to be minor [5]. First, note that the experimental values of the electric and magnetic dipole transition strengths of the  $1^-$  states are reproduced accurately. This indicates that our model precisely describes the wave functions of the  $1^-$  states. Second, we should focus on the intensities of the  $E1$  transition strengths. Since  $^{14}\text{N}$  is a self-conjugate nucleus, the isospin selection rule allows only  $|\Delta T| = 1$  transitions and forbids the  $|\Delta T| = 0$  transitions [1]. In fact, the  $|\Delta T| = 0$  transitions are suppressed by an order of magnitude compared to the

TABLE III. Electric and magnetic dipole transition strengths for the  $1_1^-$  and  $1_2^-$  states [21,24–26] given in Weisskopf units. The experimental  $B(E1)$  and  $B(M1)$  values of the  $1_2^-$  state are calculated by averaging the lifetime and branching ratio reported in [21,24–26].

$J_i^\pi \rightarrow J_f^\pi$	$ \Delta T $	$B(E1)_{\text{exp}}$ [21]	$B(E1)_{\text{calc}}$
$1_1^- \rightarrow 0_1^+$	1	$1.1(5) \times 10^{-3}$	$3.2 \times 10^{-3}$
$1_1^- \rightarrow 1_1^+$	0	$1.2(7) \times 10^{-4}$	$1.8 \times 10^{-4}$
$1_1^- \rightarrow 1_2^+$	0	–	$1.5 \times 10^{-4}$
$1_2^- \rightarrow 0_1^+$	0	$2.7(4) \times 10^{-3\text{a}}$	$1.6 \times 10^{-3}$
$1_2^- \rightarrow 1_1^+$	1	$4.4(6) \times 10^{-2\text{a}}$	$3.6 \times 10^{-2}$
$1_2^- \rightarrow 1_2^+$	1	$5.4(9) \times 10^{-2\text{a}}$	$3.4 \times 10^{-2}$
$J_i^\pi \rightarrow J_f^\pi$	$ \Delta T $	$B(M1)_{\text{exp}}$	$B(M1)_{\text{calc}}$
$1_1^- \rightarrow 0_1^-$	0	–	0.01
$1_1^- \rightarrow 2_1^-$	0	–	0.06
$1_2^- \rightarrow 0_1^-$	1	$0.37(5)^\text{a}$	0.36
$1_2^- \rightarrow 1_1^-$	1	$1.9(2)^\text{a}$	1.6
$1_2^- \rightarrow 2_1^-$	1	$0.13(3)^\text{a}$	0.17

<sup>a</sup>Calculated from the life of the  $1_2^- \rightarrow 1_1^+$  transition [24] and the averaged branching ratio of the  $1_2^-$  state given in Table 5 of Ref. [26].

$|\Delta T| = 1$  transitions for both observed and calculated values. At the same time, the nonzero values for the  $|\Delta T| = 0$  transitions indicate the isospin mixing in the  $1_1^-$  and  $1_2^-$  states. Renan *et al.* [4] estimated the mixing ratio from the  $E1$  transition probabilities. They assumed that the  $1_{1,2}^+$  and  $0_1^+$  states have no isospin mixing and the  $1_{1,2}^-$  states are admixtures of two components as follows:

$$\Psi(1_1^-) = \alpha\Phi(1) + \beta\Phi(0), \quad (9)$$

$$\Psi(1_2^-) = \beta\Phi(1) - \alpha\Phi(0), \quad (10)$$

where  $\Phi(0)$  and  $\Phi(1)$  denote the  $T = 0$  and 1 wave functions. Then, the ratio of the allowed and forbidden transitions yields the following estimate of the mixing ratio:

$$\frac{B(E1)_{\text{forbidden}}}{B(E1)_{\text{allowed}}} = \frac{\alpha^2}{\beta^2} = \frac{\alpha^2}{1 - \alpha^2}. \quad (11)$$

Applying the observed  $1_2^- \rightarrow 1_1^+$  and  $1_2^- \rightarrow 0_1^+$  transition strengths, we obtain an estimate of  $\alpha_{\text{exp}}^2 = 0.052$ , whereas our calculated transition strengths yield  $\alpha_{\text{calc}}^2 = 0.042$ , both of which are close to the mixing ratio directly calculated from our  $1^-$  wave functions ( $\alpha^2 = 0.047$  for  $1_1^-$  and 0.041 for  $1_2^-$ ). Other combinations of the transition strengths also suggest similar values; for example, the  $1_1^- \rightarrow 1_1^+$  and  $1_1^- \rightarrow 0_1^+$  transitions yield  $\alpha_{\text{exp}}^2 = 0.09$  and  $\alpha_{\text{calc}}^2 = 0.053$ .

To understand the origin of isospin mixing, we investigate the spectroscopic factors and overlap functions. We calculate the overlap between the wave function of  $^{14}\text{N}$  with the spin-parity  $J^{\pi'}$  and that of  $^{13}\text{N}$  with  $J^\pi$  [27]:

$$\varphi(\mathbf{r}) = \sqrt{13} \langle \Psi_{M'-m}^{J^\pi}({}^{13}\text{N}) | \Psi_{M'}^{J^{\pi'}}({}^{14}\text{N}) \rangle. \quad (12)$$

The overlap function is given as the multipole decomposition of  $\varphi(\mathbf{r})$ ,

$$\varphi_{jl}(r) = \int d\hat{r} [Y_l(\hat{r}) \times \chi_{1/2}]_{jm}^\dagger \varphi(\mathbf{r}), \quad (13)$$

which is the radial wave function of a valence neutron in the  $J^\pi \otimes v(l_j)$  channel. The spectroscopic factor is the norm of  $\varphi_{jl}(r)$ ,

$$S(J^\pi \otimes v(l_j)) = \int r^2 dr |\varphi_{jl}(r)|^2. \quad (14)$$

The spectroscopic factors in the  $J^\pi \otimes \pi(l_j)$  channels (the overlap between  $^{14}\text{N}$  and  $^{13}\text{C}$ ) are also calculated in the same manner. The calculated spectroscopic factors and the overlap functions of the  $1^-$  states are given in Table IV and Fig. 3, respectively. For comparison, we also present spectroscopic factors for the  $1_1^+(T = 0)$  and  $0_1^+(T = 1)$  states, which have no isospin mixing. If we assume that both  $^{13}\text{C}$  and  $^{13}\text{N}$  are the eigenstates of isospin with  $T = 1/2$ , which is a reasonable assumption indeed, the spectroscopic factors in the  $J^\pi \otimes v(l_j)$  and  $J^\pi \otimes \pi(l_j)$  channels should be equal for the pure  $T = 0$  or 1 states. In fact, we found that the equality holds for the low-lying  $1_1^+$  and  $0_1^+$  states. However, the spectroscopic factors for the  $1_1^-$  and  $1_2^-$  states show significant asymmetry between two channels because of the isospin mixing. The  $1_1^-$  state has a larger contribution from the  $1/2^- \otimes \pi(s_{1/2})$  and  $1/2^+ \otimes \nu(p_{1/2})$  channels than from the  $1/2^- \otimes \nu(s_{1/2})$

TABLE IV. Spectroscopic factors of the  $1_1^+$ ,  $0_1^+$ , and  $1_{1,2}^-$  states in the  $J^\pi \otimes \nu(l_j)$  and  $J^\pi \otimes \pi(l_j)$  channels, where  $J^\pi$  denotes the spin-parity of  $^{14}\text{N}$  and  $^{14}\text{C}$  and  $l_j$  denotes the orbital and total angular momenta of a valence neutron or proton.

$1_1^+$	$\frac{1}{2}^- \otimes \nu(p_{1/2})$	$\frac{1}{2}^- \otimes \pi(p_{1/2})$	$\frac{5}{2}^- \otimes \nu(p_{3/2})$	$\frac{5}{2}^- \otimes \pi(p_{3/2})$
	0.87	0.87	1.28	1.29
$0_1^+$	$\frac{1}{2}^- \otimes \nu(p_{1/2})$	$\frac{1}{2}^- \otimes \pi(p_{1/2})$	$\frac{3}{2}^- \otimes \nu(p_{3/2})$	$\frac{3}{2}^- \otimes \pi(p_{3/2})$
	0.90	0.90	0.99	1.04
$1_1^-$	$\frac{1}{2}^- \otimes \nu(s_{1/2})$	$\frac{1}{2}^- \otimes \pi(s_{1/2})$	$\frac{1}{2}^+ \otimes \nu(p_{1/2})$	$\frac{1}{2}^+ \otimes \pi(p_{1/2})$
	0.23	0.43	0.47	0.25
$1_2^-$	$\frac{1}{2}^- \otimes \nu(s_{1/2})$	$\frac{1}{2}^- \otimes \pi(s_{1/2})$	$\frac{1}{2}^+ \otimes \nu(p_{1/2})$	$\frac{1}{2}^+ \otimes \pi(p_{1/2})$
	0.38	0.23	0.28	0.42

and  $1/2^+ \otimes \pi(p_{1/2})$  channels, whereas the  $1_2^-$  state shows the opposite trend.

The origin of the asymmetry may be understood as follows. Notice that  $^{13}\text{N}(1/2^+)$  and  $^{13}\text{C}(1/2^+)$  are approximated as the  $\pi(s_{1/2})$  and  $\nu(s_{1/2})$  states on top of the  $^{12}\text{C}$  ground state as an inert core. Thus, the  $\pi(s_{1/2})$  and  $\nu(s_{1/2})$  orbits are always implicated in the dominant component of the  $1_{1,2}^-$  states. Furthermore, Table IV indicates that the proton excitation into the  $\pi(s_{1/2})$  orbit has a larger probability than the neutron excitation into  $\nu(s_{1/2})$  for the  $1_1^-$  state, and the opposite is true for the  $1_2^-$  state. This indicates that the proton excitation into the  $\pi(s_{1/2})$  orbit is energetically favored over the neutron excitation. Consequently, the symmetry between protons and neutrons is broken, leading to the isospin mixing. We consider that this asymmetry originates from the Coulomb energy. As shown in Fig. 3, the  $\pi(s_{1/2})$  orbit is spatially extended as compared to  $\pi(p_{1/2})$  as it is close to the threshold energy. Consequently,  $\pi(s_{1/2})$  has smaller Coulomb repulsion than  $\pi(p_{1/2})$  and  $\pi(p_{3/2})$ , and hence, the single-particle excitation energy for proton excitation is smaller than that for neutron excitation. We also found that other excited states with isospin mixing such as the  $2_{1,2,3}^+$ ,  $2_{2,3}^-$ , and  $3_{2,3}^-$  states always involve the single-particle excitation to  $s_{1/2}$ . Therefore, we conclude that the Coulomb energy shift of the proton  $s_{1/2}$  orbit is a major source of the isospin mixing in the excited states close to the proton and neutron decay thresholds.

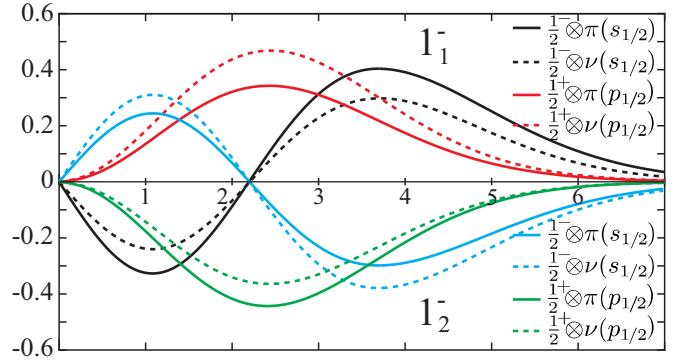


FIG. 3. Overlap functions of the  $1_1^+$ ,  $0_1^+$ , and  $1_{1,2}^-$  states in the  $J^\pi \otimes \nu(l_j)$  and  $J^\pi \otimes \pi(l_j)$  channels. The phases of the overlap functions are arbitrarily chosen for presentation.

#### IV. SUMMARY

In this work, we proposed a tractable method to describe the isospin mixing within the framework of GCM. By applying the Fermi transition operator to the wave functions of isobars, we generated the wave functions of the isobaric analog states, which are used as the basis of GCM calculations. We have applied this method to  $^{14}\text{N}$  and demonstrated that it plausibly describes both the  $T = 0$  and 1 states and their mixing. We have also discussed that our model reasonably describes the strengths of the allowed and forbidden  $E1$  transitions that are consistent with the mixing ratio. Furthermore, based on the spectroscopic factors and overlap functions, we deduced that the Coulomb energy shift of the  $s_{1/2}$  orbit is a major source of the isospin mixing.

#### ACKNOWLEDGMENTS

We thank Prof. D. J. Millener for his help in improving this work, especially in updating the observed electromagnetic transition strength to the latest evaluation. This work was supported by JSPS KAKENHI Grant No. 19K03859. A part of the numerical computation was conducted at the Yukawa Institute Computer Facility.

[1] E. K. Warburton and J. Weneser, in *Isospin in Nuclear Physics*, edited by D. H. Wilkinson (North-Holland, Amsterdam, 1969)  
 [2] A. Bohr and B. Mottelson, *Nuclear Structure Vol. 1* (Benjamin, New York, 1969).  
 [3] F. C. Barker, *Nucl. Phys.* **83**, 418 (1966).  
 [4] M. J. Renan, J. P. Sellschop, R. J. Keddy, and D. W. Mingay, *Nucl. Phys. A* **193**, 470 (1972).  
 [5] P. Descouvemont and D. Baye, *Nucl. Phys. A* **459**, 374 (1986).  
 [6] C. Rolfs and W. Rodney, *Cauldrons in the Cosmos: Nuclear Astrophysics*, Rolfs, Rodney (University of Chicago Press, Chicago, 1988).  
 [7] S. E. Woosley, A. Heger, and T. A. Weaver, *Rev. Mod. Phys.* **74**, 1015 (2002).  
 [8] P. Descouvemont and D. Baye, *Phys. Rev. C* **36**, 1249 (1987).

[9] R. J. Deboer, J. Görres, M. Wiescher, R. E. Azuma, A. Best, C. R. Brune, C. E. Fields, S. Jones, M. Pignatari, D. Sayre, K. Smith, F. X. Timmes, and E. Uberseder, *Rev. Mod. Phys.* **89**, 035007 (2017).  
 [10] W. Satuła and R. Wyss, *Phys. Rev. Lett.* **86**, 4488 (2001).  
 [11] K. Sato, J. Dobaczewski, T. Nakatsukasa, and W. Satuła, *Phys. Rev. C* **88**, 061301(R) (2013).  
 [12] Y. Kanada-En'yo, H. Morita, and F. Kobayashi, *Phys. Rev. C* **91**, 054323 (2015).  
 [13] P. Bączyk, J. Dobaczewski, M. Konieczka, W. Satuła, T. Nakatsukasa, and K. Sato, *Phys. Lett. B* **778**, 178 (2018).  
 [14] W. Satuła, J. Dobaczewski, W. Nazarewicz, and M. Rafalski, *Phys. Rev. C* **81**, 054310 (2010).  
 [15] H. Morita and Y. Kanada-En'yo, *Prog. Theor. Exp. Phys.* **2016**, 103D02 (2016).

- [16] J. F. Berger, M. Girod, and D. Gogny, *Comput. Phys. Commun.* **63**, 365 (1991).
- [17] M. Kimura, *Phys. Rev. C* **69**, 044319 (2004).
- [18] D. L. Hill and J. A. Wheeler, *Phys. Rev.* **89**, 1102 (1953).
- [19] T. Suhara and Y. Kanada-En'yo, *Phys. Rev. C* **82**, 044301 (2010).
- [20] T. Baba and M. Kimura, *Phys. Rev. C* **94**, 044303 (2016).
- [21] F. Ajzenberg-Selove, *Nucl. Phys. A* **523**, 1 (1991).
- [22] F. Ajzenberg-Selove, *Nucl. Phys. A* **360**, 1 (1981).
- [23] N. J. Stone, *At. Data Nucl. Data Tables* **90**, 75 (2005).
- [24] J. D. King, R. E. Azuma, J. B. Vise, J. Görres, C. Rolfs, H. P. Trautvetter, and A. E. Vlieks, *Nucl. Phys. A* **567**, 354 (1994).
- [25] V. J. Zeps, E. G. Adelberger, A. García, C. A. Gossett, H. E. Swanson, W. Haerberli, P. A. Quin, and J. Sromicki, *Phys. Rev. C* **51**, 1494 (1995).
- [26] J. Kiener, M. Gros, V. Tatischeff, D. Attié, I. Bailly, A. Bauchet, C. Chapuis, B. Cordier, I. Deloncle, M. G. Porquet, S. Schanne, N. De Séréville, and G. Tauzin, *Nucl. Instrum. Methods Phys. Res. A* **519**, 623 (2004).
- [27] M. Kimura, *Phys. Rev. C* **95**, 034331(2017).